THE JOURNAL OF PHYSICAL CHEMISTRY C

Article

Cite This: J. Phys. Chem. C 2019, 123, 28893−28897

pubs.acs.org/JPCC

Effects of Material Dimensionality on the Optical Properties of $CsPbBr_3$ Nanomaterials

Xuanyu Zhang,[†] Xian Gao,[‡] Guotao Pang,[‡] Tingchao He,[§] Guichuan Xing,*[,∥] and Rui Chen*[,‡]

[†]Key Laboratory of Flexible Electronics and Institute of Advanced Materials, Jiangsu National Synergetic Innovation Center for Advanced Materials, Nanjing Tech University, 30 South Puzhu Road, Nanjing 211816, P. R. China

[‡]Department of Electrical and Electronic Engineering, Southern University of Science and Technology, Shenzhen 518055, P. R. China

[§]College of Physics and Optoelectronic Engineering, Shenzhen University, Shenzhen 518060, P. R. China

[∥]The Institute of Applied Physics and Materials Engineering, University of Macau, Avenida da Universidade, Taipa, Macau, P. R. China

ABSTRACT: Inorganic perovskites such as $CsPbBr_3$ have attracted intensive research attention due to their excellent thermal stability and high photoluminescence quantum efficiency. With the decrease of the material's dimension, quantum confinement effects will take place, which will induce many interesting properties. Here, quasi two-dimensional perovskite nanoplatelets (NPLs) and three-dimensional perovskite nanocrystals (NCs) have been grown, and their optical properties have been compared and discussed. It is interesting to find that the photon energy of $CsPbBr_3$ NPLs hardly changes with temperature due to strong electron−phonon interaction. At the same time, the strong quantum confinement effect results in a smaller Stokes shift and a faster fluorescence lifetime. In addition, although the NPLs have many surface defects, they exhibit a relatively strong negative thermal quenching effect of emission. These results demonstrate the unique optical properties of perovskite NPLs that can pave the way for future nanoscale devices.

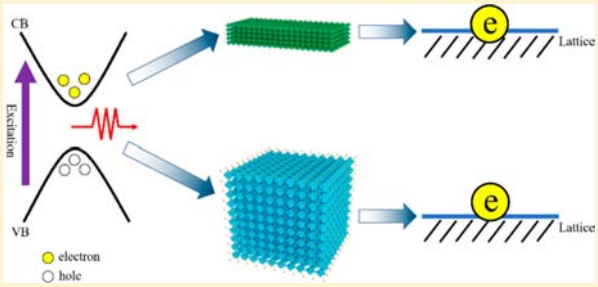

INTRODUCTION

Due to the special crystal structure of ABX_3 (A = organic ammonium cation or inorganic metal cation, B = Pb^{2+} or Sn^{2+}, X = halogen anion), perovskite materials possess unique electrical and optical properties which have attracted intensive research interest for many optoelectronic devices applications,[1,2] such as photodetectors,[3,4] light-emitting diodes (LEDs),[5] and lasers.[6] The nearly perfect photovoltaic properties of organic−inorganic hybrid perovskites have been witnessed in the past few years. For example, the power conversion efficiency of the perovskite solar cell has increased from 3.8%[7] to 25.2%,[8] which is comparable to that of monocrystalline silicon-based solar cells.[9] Compared to organic−inorganic hybrid perovskites,[10,11] inorganic perovskites such as $CsPbX_3$ (X = Cl, Br, or I) demonstrate higher luminescence quantum yield up to 90%[12,13] and narrower emission bandwidth and higher stability, which make them promising candidates as new materials for light-emitting diodes (LEDs). It is well-known that in addition to material composition, the dimension of material not only influences their chemical properties but also determines their optical and electronic properties for a wide variety of applications.[14] For example, Brumberg et al. showed that the electron transfer rate from $CsPbBr_3$ to CdSe in two-dimensional (2D) materials is faster than that in zero dimensional (0D) materials.[15] The other report also shows that compared with the spherical nuclear system (0D),[16] the efficiency of Förster resonance energy transfer (FRET) in the nanorod system (1D) had been greatly improved. In addition, Asaf Salant et al. used higher dimensional nanorods (NRs) to replace quantum dots (QDs) as sensitizers in the sensitized solar cells,[17] which improved the charge injection from CdSe to TiO_2, and the charge recombination was significantly suppressed. The modification of material's dimension will lead to the change of energy bands as well as band alignment, which will further influence the optical recombination. These findings offer potential implications for the design of advanced optoelectronic devices.[18,19]

However, up until now, many studies have focused on the investigation of $CsPbBr_3$ colloidal QDs,[20] nanocrystals (NCs),[21] and thin films,[22] while little research has been devoted to the luminescence of $CsPbBr_3$ nanoplatelets (NPLs). For quasi 2D NPLs materials, the strong quantum confinement effect allows them to emit blue light, which is quite different from perovskite $CsPbBr_3$ with other shapes. Although the effects of dimensionality and composition on the linear and nonlinear optics properties of the $CsPbBr_xI_{3-x}$ perovskite have been reported recently,[23] there is no in-depth study on the unique optical properties of NPLs. Here, in

Received: September 10, 2019
Revised: November 3, 2019
Published: November 4, 2019

DOI: 10.1021/acs.jpcc.9b08606
J. Phys. Chem. C 2019, 123, 28893−28897

order to study the optical properties caused by the dimensions, we prepared $CsPbBr_3$ NPLs and NCs samples with similar lateral sizes, respectively. By comparing the room temperature and temperature-dependent photoluminescence (PL) spectra of $CsPbBr_3$ nanomaterials with different dimensions, the optical properties of NPLs were analyzed and discussed. Regarding the optical emission, it is found that the competition between electron−phonon interaction and thermal expansion is comparable for NPLs, while it is stronger in the case of NCs. This causes the photon energy of NPLs to hardly change with temperature, which further leads to a better thermal color purity of the materials. Meanwhile, there are more defects in NPLs, which leads to a stronger negative thermal quenching phenomenon. Our research has theoretical guiding significance for the application of two-dimensional nanomaterials in the design of perovskite optoelectronic devices.

EXPERIMENTAL SECTION

Sample Preparation. $CsPbBr_3$ NPLs and NCs were fabricated according to the procedures published in refs 14 and 24 with slight modifications. All samples were fabricated by drop-casting of $CsPbBr_3$ NPLs and NCs solutions on quartz substrates. All the measurements were performed under film conditions.

Morphology Characterization. A transmission electron microscope (TEM; Talos F200X) was used to characterize the morphology and size of the NPLs and NCs. TEM samples were prepared through dropping NPLs and NCs solution with relatively dilute concentration on carbon-coated 200 mesh copper TEM grids.

Steady-State Optical Measurement. Measurements for absorption and absolute photoluminescence quantum yields (PLQY) were performed by a UV−vis−NIR spectrophotometer (Lambda 950, PerkinElmer, Inc.) and a spectrometer (Zolix, SENS-9000), respectively. $CsPbBr_3$ NPLs and NCs samples were placed inside a closed-cycle helium cryostat with quartz windows for PL measurements. The PL spectra were recorded using a charge-coupled device (CCD). A 325 nm continuous wave (CW) He−Cd gas laser was used as the excitation source. The temperature during the PL measurement is well-controlled from 50 to 295 K.

PL Lifetime Measurement. Time-resolved PL experiments were carried out at room temperature. The excitation source was a pulsed ultraviolet picosecond diode laser operating at 375 nm. The pulse width and repetition rate of the laser were 40 ps and 20 MHz, respectively. The signal was dispersed by a 320 mm monochromator (iHR320 from Horiba, Ltd.) combined with suitable filters and detected based on the time-correlated single photon counting (TCSPC) technique.

RESULTS AND DISCUSSION

The representative TEM images of $CsPbBr_3$ NPLs and NCs are shown in parts a and b of Figure 1, respectively. It can be seen that the NPLs and NCs are both with high uniformity. As shown in Figure 1a, the lateral area and thickness of the NPLs can be clearly seen. The average lateral size of $CsPbBr_3$ NPLs is about 18.2 nm, and the thickness is around 3.5 nm, which corresponds to four monolayers. In comparison, the NCs possess cubic shapes and the size is around 15 nm determined based on Figure 1b. From the images, it can be clearly seen that the lateral sizes of NPLs and NCs are similar. However,

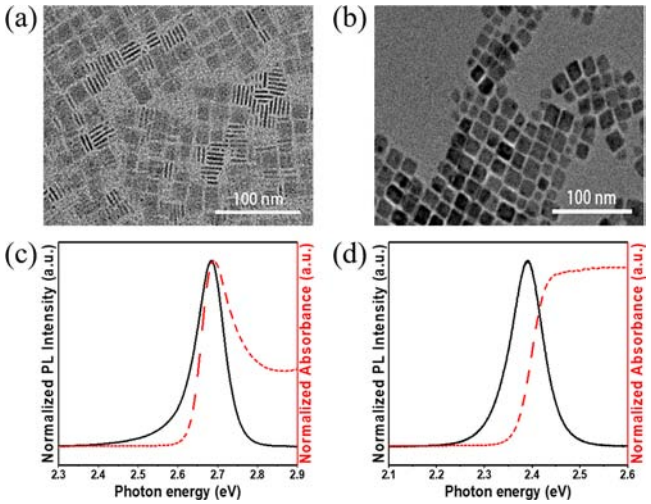

Figure 1. (a, b) Transmission electron microscopy (TEM) image of inorganic perovskite NPLs and NCs films. (c, d) Absorption (dashed line) and photoluminescence (solid line) spectra at room temperature of NPLs and NCs, respectively.

NPLs are much thinner than NCs in the *z*-direction with thickness comparable to their exciton Bohr radius (3.5 nm) of the $CsPbBr_3$ bulk crystal. Therefore, it is expected that NPLs have a stronger quantum confinement effect. In addition, we can see from Figure 1a that the synthesized NPLs are dispersed and do not self-assemble into thicker platelets or even bulk phases as reported in the literature.[25,26] Therefore, the accuracy of the experimental data can be ensured during the measurements.

Parts c and d of Figure 1 show the normalized UV−visible absorption and PL emission of $CsPbBr_3$ NPLs and NCs, respectively. It can be seen that $CsPbBr_3$ NPLs exhibit a very clear exciton absorption peak at 2.69 eV, while a poorly resolved absorption edge of NCs was observed at 2.45 eV, which is perhaps related to the inhomogeneous size distribution.[27] Strong PL emission can be observed at 2.68 and 2.38 eV for NPLs and NCs, respectively. For $CsPbBr_3$ NPLs and NCs, the full width at half-maximum (fwhm) of the emission were 82.3 and 79.4 meV, respectively, which is similar to the value in the recent reports.[28,29] The narrow fwhm indicates that the samples have good size uniformity. Obviously, the Stokes shifts of 7 meV for NPLs and 57.1 meV for NCs are very different, which can be attributed to the stronger quantum confinement effects and better crystal quality of NPLs.[12,27] The smaller Stokes shift in the NPLs indicates more proportion of absorbed energy for luminescence, which is beneficial to the development of device applications. Moreover, it is worth noting that NPLs have longer PL tails than NCs, which implies a stronger electron−phonon coupling.[30,31]

The PL lifetime of NPLs and NCs are measured and the decay curves are given in parts a and b of Figure 2. Both PL decay curves can be well-fitted with a triexponential function

$$A(t) = A_1 \exp\left(-\frac{t}{\tau_1}\right) + A_2 \exp\left(-\frac{t}{\tau_2}\right) + A_3 \exp\left(-\frac{t}{\tau_3}\right) \quad (1)$$

where A, A_1, A_2, and A_3 are constants, t is time, and τ_1, τ_2, and τ_3 represent the decay lifetimes corresponding to the intrinsic exciton relaxation, the interaction between excitons and

DOI: 10.1021/acs.jpcc.9b08606
J. Phys. Chem. C 2019, 123, 28893−28897

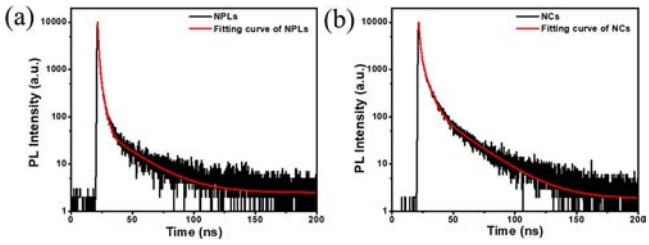

Figure 2. (a, b) PL decay curves (black lines) corresponding fitting curves (red lines) about NPLs and NCs.

phonons, and the interaction between excitons and defects, respectively. The average lifetime (τ_{ave}) can be determined to be as

$$\tau_{ave} = \frac{A_1\tau_1^2 + A_2\tau_2^2 + A_3\tau_3^2}{A_1\tau_1 + A_2\tau_2 + A_3\tau_3} \quad (2)$$

The fitting result shown in Figure 2a and the derived average lifetime (τ_{ave}) is 2.02 ns for NPLs and 4.47 ns for NCs, respectively. The values of the lifetimes reveal the ratio of radiative recombination to nonradiative transitions. The relatively small lifetime of NPLs can be ascribed to their strong quantum confinement effect, which leads to more overlapping between electron and hole wave function, and therefore a faster recombination rate has been realized. In addition, high-density surface defects and trap states in NPLs may also lead to shorter lifetimes.[32] At the same time, it is noted that the PLQY of NPLs film and NCs film were 36.8% and 43.2%, respectively. The lower value of PLQY also suggests more surface defects in NPLs. It is reasonable because the surface to volume ratio is higher in the case of NPLs.

Parts a and b of Figure 3 plot the normalized temperature-dependent PL emission of $CsPbBr_3$ NPLs and NCs,

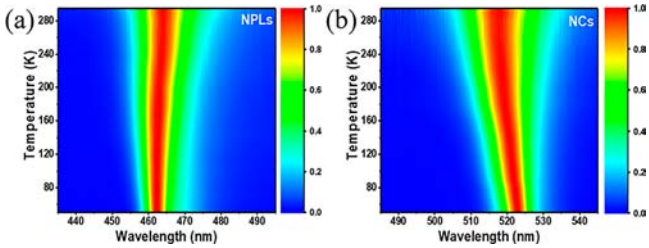

Figure 3. (a, b) Normalized PL spectra of a 2D pseudocolor plot of the NPLs and NCs at temperatures from 50 to 295 K.

respectively. It can be clearly seen that, in Figure 3a, the photon energy of NPLs does not change significantly with temperature, while the peak position of NCs gradually blueshifts as the temperature increases. This smaller change indicates that NPLs have better thermal color purity. Detail physical mechanism of the peak shift of the samples will be discussed in the lateral section.

The comparison of photon energy, fwhm and integrated PL intensity as a function of temperature are shown in parts a–d of Figure 4, respectively. Figure 4a shows the trend of photon energy versus temperature for NPLs and NCs. The difference between the two materials with different dimensions can be explained by the competition between thermal expansion and electron–phonon coupling. By assuming a linear relationship between lattice constant and temperature, the temperature

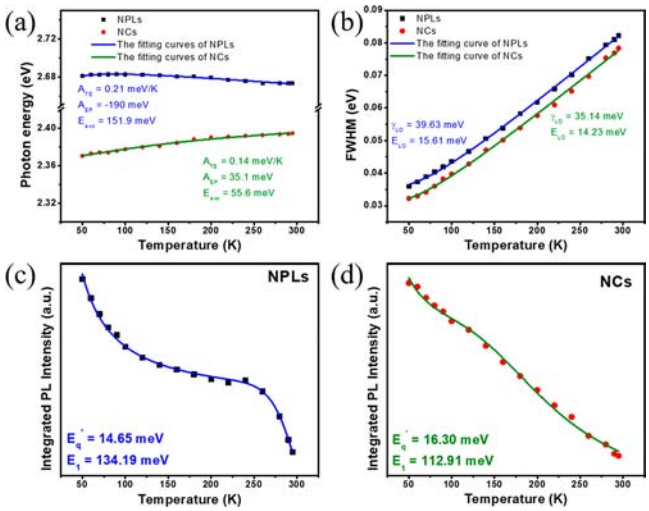

Figure 4. (a) Photon energy as a function of temperature; (b) Fwhm as a function of temperature; (c, d) Integrated PL intensity as a function of temperature of NPLs and NCs, respectively.

dependence of the PL peak energy is generally estimated by the following expression:[33]

$$E(T) = E_0 + A_{TE}T + A_{EP}\left(\frac{2}{\exp(\hbar\omega/k_BT) - 1} + 1\right) \quad (3)$$

Here E_0 is the unrenormalized bandgap, A_{TE} and A_{EP} are the weight of the thermal expansion (TE) and exciton–phonon (EP) interaction, respectively, and $\hbar\omega$ is the average optical phonon energy. Due to the quantum factor in the phonon distribution function, there is an energy correction of the bandgap even at zero temperature, namely $E_g(T = 0) = E_0 + A_{EP}$. Figure 4a shows the fitted results, and the parameters obtained are E_0 = 2.51 eV, A_{TE} = 0.21 meV/K, A_{EP} = −190.0 meV and $\hbar\omega$ = 151.9 meV for NPLs and E_0 = 2.43 eV, A_{TE} = 0.14 meV/K, A_{EP} = 35.1 meV, and $\hbar\omega$ = 55.6 meV for NCs. Obviously, the most fundamental difference lies in the contribution of electron–phonon interaction to the photon energy. In $CsPbBr_3$ NPLs, the exciton–phonon interaction has a bigger contribution than the NC, leading to the constant or even redshift of its photon energy.

Figure 4b shows the fwhm of NPLs and NCs as a function of temperature. The value of the fwhm of NPLs is always larger than that of NCs, which can be attributed to the stronger electron–phonon coupling in NPLs than NCs. The analysis of temperature-dependent emission broadening has long been used to evaluate the mechanism of exciton–phonon coupling for a large number of materials. The emission broadening can be expressed as[34]

$$\Gamma(T) = \Gamma_0 + \gamma_{LO}(e^{E_{LO}/k_BT} - 1)^{-1} \quad (4)$$

where Γ_0 is about the temperature-independent inhomogeneous broadening, which results from the disorder and imperfection scattering. The second term is the homogeneous broadening term, which arises from longitudinal optical (LO) phonon-charge scattering. γ_{LO} and E_{LO} are electron–phonon coupling strength and the LO phonon energy, respectively. By using eq 4, the fitted curve of the temperature dependent fwhm versus temperature was plotted in Figure 4c, yielding the coupling strength γ_{LO} = 39.6 meV and an average phonon

DOI: 10.1021/acs.jpcc.9b08606
J. Phys. Chem. C 2019, 123, 28893−28897

energy of E_{LO} = 15.6 meV for NPLs, and γ_{LO} = 35.1 meV and an average phonon energy of E_{LO} = 14.2 meV for NCs, respectively. The LO phonon energy of NPLs is a little larger than NCs, which is consistent with previous literature reports.[35] Exploring exciton−phonon interactions in perovskite nanomaterials is indispensable because the proper understanding about the interaction between carriers and lattice vibrations (phonons) is a prerequisite for the fabrication of optoelectronic devices.

Parts c and d of Figure 4 plot the integrated PL intensity of NPLs and NCs against temperature, respectively. In Figure 4c, the decrease of the emission intensity from NPLs is very slow in the temperature range from 120 to 240 K, and after 240 K, the intensity begins to decrease rapidly. The emission intensity from NCs decreases faster with temperature compared to NPLs. It is clearly observed that the PL intensity of NPLs shows a negative thermal quenching at high temperatures, which has been observed in many semiconductors and has been attributed to either delocalization of carriers or quenching of the nonradiative defects. It has been reported that more defects will lead to more significant negative thermal quenching.[36] It can be described by a modified expression[28,37]

$$I(T) = I(0)\frac{1 + \sum_{q=1}^{w} D_q \exp(-E_q'/k_B T)}{1 + \sum_{j=1}^{m} C_j T^{2} \exp(-E_j/k_B T)} \quad (5)$$

where E_q' describes the activation energies for processes that increases the PL intensity with increasing temperature. The fitted result shown in Figure 4c gives E_1 = 134.2 meV for $CsPbBr_3$ NPLs film (which is consistent with the exciton binding energy) and E_q' = 14.7 meV. For NCs film, the obtained E_1 = 112.9 meV and E_q' = 16.3 meV. Strong quantum confinement effect can increase the overlap between electron and hole wave functions, which further increase the exciton binding energy of the material.[38,39] Therefore, the exciton binding energy (E_b) in NPLs is bigger than in NCs. The higher E_b value indicates that the excitons are highly stable and the probability for their dissociation is less, in particular at temperatures T < 300 K. The fitted results are consistent with the discussion above, that is, NPLs has a larger exciton binding energy and shallower defect levels.

CONCLUSIONS

In summary, we have investigated the effects of material's dimension on the optical properties of $CsPbBr_3$ in forms of NPLs and NCs, respectively. The more obviously exciton absorption was found in NPLs suggesting that the exciton binding energy is larger than that of NCs. Meanwhile, the shorter lifetime of NPLs is more suitable for optoelectronic devices such as photodetector or modulator. In addition, due to the stronger electron−phonon interaction in quasi 2D material system, $CsPbBr_3$ NPLs exhibit almost unchanged photon energy at various temperatures below 300 K. Although perovskite with quasi 2D geometry provides a larger specific surface area which leads to more surface defects, the negative thermal quenching effect of NPLs is more pronounced with temperature increasing. This work demonstrates the unique optical properties of perovskite nanoplatelets, which facilitates the application of devices.

AUTHOR INFORMATION

Corresponding Authors

*(G.X.) E-mail: gcxing@um.edu.mo.

*(R.C.) E-mail: chenr@sustech.edu.cn.

ORCID

Rui Chen: 0000-0002-0445-7847

Author Contributions

The manuscript was written through contributions of all authors. All authors have given approval to the final version of the manuscript.

Notes

The authors declare no competing financial interest.

ACKNOWLEDGMENTS

This work is supported by the National Natural Science Foundation of China (11574130), Shenzhen Science and Technology Innovation Commission (Projects Nos. KQJSCX20170726145748464, JCYJ20180305180553701, and KQTD2015071710313656). G.X. acknowledges financial support from The Science and Technology Development Fund (File No. 091/2017/A2), a research grant (MYRG2018-00148-IAPME) from University of Macau, and the National Natural Science Foundation of China (91733302, 61605073, and 2015CB932200).

REFERENCES

(1) Dou, L.; Yang, Y.; You, J.; Hong, Z.; Chang, W. H.; Li, G.; Yang, Y. Solution-Processed Hybrid Perovskite Photodetectors with High Detectivity. *Nat. Commun.* **2014**, *5*, 5404.

(2) Saidaminov, M. I.; Haque, M. A.; Savoie, M.; Abdelhady, A. L.; Cho, N.; Dursun, I.; Buttner, U.; Alarousu, E.; Wu, T.; Bakr, O. M. Perovskite Photodetectors Operating in Both Narrowband and Broadband Regimes. *Adv. Mater.* **2016**, *28*, 8144−8149.

(3) Adinolfi, V.; Ouellette, O.; Saidaminov, M. I.; Walters, G.; Abdelhady, A. L.; Bakr, O. M.; Sargent, E. H. Fast and Sensitive Solution-Processed Visible-Blind Perovskite UV Photodetectors. *Adv. Mater.* **2016**, *28*, 7264−7268.

(4) Fang, Y.; Dong, Q.; Shao, Y.; Yuan, Y.; Huang, J. Highly Narrowband Perovskite Single-Crystal Photodetectors Enabled by Surface-charge Recombination. *Nat. Photonics* **2015**, *9*, 679−686.

(5) Liang, D.; Peng, Y.; Fu, Y.; Shearer, M. J.; Zhang, J.; Zhai, J.; Zhang, Y.; Hamers, R. J.; Andrew, T. L.; Jin, S. Color-Pure Violet-Light-Emitting Diodes Based on Layered Lead Halide Perovskite Nanoplates. *ACS Nano* **2016**, *10*, 6897−6904.

(6) Zhu, H.; Fu, Y.; Meng, F.; Wu, X.; Gong, Z.; Ding, Q.; Gustafsson, M. V.; Trinh, M. T.; Jin, S.; Zhu, X. Lead Halide Perovskite Nanowire Lasers with Low Lasing Thresholds and High Quality Factors. *Nat. Mater.* **2015**, *14*, 636−642.

(7) Kojima, A.; Teshima, K.; Shirai, Y.; Miyasaka, T. Organometal Halide Perovskites as Visible-Light Sensitizers for Photovoltaic Cells. *J. Am. Chem. Soc.* **2009**, *131*, 6050−6051.

(8) Jiang, Q.; Zhao, Y.; Zhang, X.; Yang, X.; Chen, Y.; Chu, Z.; Ye, Q.; Li, X.; Yin, Z.; You, J. Surface Passivation of Perovskite Film for Efficientsolar Cells. *Nat. Photonics* **2019**, *13*, 460−466.

(9) Green, M. A. The Path to 25% Silicon Solar Cell Efficiency: History of Silicon Cell Evolution. *Prog. Photovoltaics* **2009**, *17*, 183−189.

(10) Sedighi, R.; Tajabadi, F.; Shahbazi, S.; Gholipour, S.; Taghavinia, N. Mixed-Halide $CH_3NH_3PbI_{3-x}X_x$ (X = Cl, Br, I) Perovskites: Vapor-Assisted Solution Deposition and Application as Solar Cell Absorbers. *ChemPhysChem* **2016**, *17*, 2382−2388.

(11) Alkorta, I.; Elguero, J. A Theoretical Study of Perovskites Related to $CH_3NH_3PbX_3$ (X = F, Cl, Br, I). *New J. Chem.* **2018**, *42*, 13889−13898.

(12) Koscher, B. A.; Swabeck, J. K.; Bronstein, N. D.; Alivisatos, A. P. Essentially Trap-Free $CsPbBr_3$ Colloidal Nanocrystals by Post-Synthetic Thiocyanate Surface Treatment. *J. Am. Chem. Soc.* **2017**, *139*, 6566−6569.

DOI: 10.1021/acs.jpcc.9b08606
J. Phys. Chem. C 2019, 123, 28893−28897

(13) Xuan, T.; Yang, X.; Lou, S.; Huang, J.; Liu, Y.; Yu, J.; Li, H.; Wong, K. L.; Wang, C.; Wang, J. Highly Stable $CsPbBr_3$ Quantum Dots Coated with Alkyl Phosphate for White Light-Emitting Diodes. *Nanoscale* **2017**, *9*, 15286−15290.
(14) Liang, Z.; Zhao, S.; Xu, Z.; Qiao, B.; Song, P.; Gao, D.; Xu, X. Shape-Controlled Synthesis of All-Inorganic $CsPbBr_3$ Perovskite Nanocrystals with Bright Blue Emission. *ACS Appl. Mater. Interfaces* **2016**, *8*, 28824−28830.
(15) Brumberg, A.; Diroll, B. T.; Nedelcu, G.; Sykes, M. E.; Liu, Y.; Harvey, S. M.; Wasielewski, M. R.; Kovalenko, M. V.; Schaller, R. D. Material Dimensionality Effects on Electron Transfer Rates Between $CsPbBr_3$ and CdSe Nanoparticles. *Nano Lett.* **2018**, *18*, 4771−4776.
(16) Halivni, S.; Sitt, A.; Hadar, I.; Banin, U. Effect of Nanoparticle Dimensionality on Fluorescence Resonance Energy Transfer in Nanoparticle−Dye Conjugated Systems. *ACS Nano* **2012**, *6*, 2758−2765.
(17) Salant, A.; Shalom, M.; Tachan, Z.; Buhbut, S.; Zaban, A.; Banin, U. Quantum Rod-Sensitized Solar Cell: Nanocrystal Shape Effect on the Photovoltaic Properties. *Nano Lett.* **2012**, *12*, 2095−2100.
(18) Liu, R.; Bloom, B. P.; Waldeck, D. H.; Zhang, P.; Beratan, D. N. Controlling the Electron-Transfer Kinetics of Quantum-Dot Assemblies. *J. Phys. Chem. C* **2017**, *121*, 14401−14412.
(19) Gur, I.; Fromer, N. A.; Chen, C. P.; Kanaras, A. G.; Alivisatos, A. P. Hybrid Solar Cells with Prescribed Nanoscale Morphologies Based on Hyperbranched Semiconductor Nanocrystals. *Nano Lett.* **2007**, *7*, 409−414.
(20) Liu, X.; Kuang, W.; Ni, H.; Tao, Z.; Huang, Q.; Chen, J.; Liu, Q.; Chang, J.; Lei, W. Highly Sensitive and Fast Graphene Nanoribbons/$CsPbBr_3$ Quantum Dots Phototransistor with Enhanced Vertically Metal Oxide Heterostructures. *Nanoscale* **2018**, *10*, 10182−10189.
(21) Swarnkar, A.; Chulliyil, R.; Ravi, V. K.; Irfanullah, M.; Chowdhury, A.; Nag, A. Colloidal $CsPbBr_3$ Perovskite Nanocrystals: Luminescence beyond Traditional Quantum Dots. *Angew. Chem., Int. Ed.* **2015**, *54*, 15424−15428.
(22) Li, C.; Zang, Z.; Han, C.; Hu, Z.; Tang, X.; Du, J.; Leng, Y.; Sun, K. Enhanced Random Lasing Emission from Highly Compact $CsPbBr_3$ Perovskite Thin Films Decorated by ZnO Nanoparticles. *Nano Energy* **2017**, *40*, 195−202.
(23) Zhao, F.; Li, J.; Gao, X.; Qiu, X.; Lin, X.; He, T.; Chen, R. Comparison Studies of the Linear and Nonlinear Optical Properties of $CsPbBr_xI_{3-x}$ Nanocrystals: The Influence of Dimensionality and Composition. *J. Phys. Chem. C* **2019**, *123*, 9538−9543.
(24) Akkerman, Q.; Motti, S. G.; Srimath Kandada, A. R.; Mosconi, E.; D'Innocenzo, V.; Bertoni, G.; Marras, S.; Kamino, B. A.; Miranda, L.; De Angelis, F.; et al. Solution Synthesis Approach to Colloidal Cesium Lead Halide Perovskite Nanoplatelets with Monolayer-Level Thickness Control. *J. Am. Chem. Soc.* **2016**, *138*, 1010−1016.
(25) Wang, Y.; Li, X.; Sreejith, S.; et al. Photon Driven Transformation of Cesium Lead Halide Perovskites from Few-Monolayer Nanoplatelets to Bulk Phase. *Adv. Mater.* **2016**, *28*, 10637−10643.
(26) Peng, L.; Geng, J.; Ai, L.; Zhang, Y.; Xie, R.; Yang, W. Room Temperature Synthesis of Ultra-Small, Near-Unity Single-Sized Lead Halide Perovskite Quantum Dots with Wide Color Emission Tunability, High Color Purity and High Brightness. *Nanotechnology* **2016**, *27*, 335604.
(27) Yuan, X.; Hou, X.; Li, J.; Qu, C.; Zhang, W.; Zhao, J.; Li, H. Thermal Degradation of Luminescence in Inorganic Perovskite $CsPbBr_3$ Nanocrystals. *Phys. Chem. Chem. Phys.* **2017**, *19*, 8934−8940.
(28) Li, J.; Luo, L.; Huang, H.; Ma, C.; Ye, Z.; Zeng, J.; He, H. 2D Behaviors of Excitons in Cesium Lead Halide Perovskite Nanoplatelets. *J. Phys. Chem. Lett.* **2017**, *8*, 1161−1168.
(29) Li, J.; Yuan, X.; Jing, P.; Li, J.; Wei, M.; Hua, J.; Zhao, J.; Tian, L. Temperature-Dependent Photoluminescence of Inorganic Perovskite Nanocrystal Films. *RSC Adv.* **2016**, *6*, 78311−78316.
(30) Chen, R.; Ye, Q.; He, T.; Wu, T.; Sun, H. Uniaxial Tensile Strain and Exciton−Phonon Coupling in Bent ZnO Nanowires. *Appl. Phys. Lett.* **2011**, *98*, 423−426.
(31) Lao, X.; Yang, Z.; Su, Z.; Bao, Y.; Zhang, J.; Wang, X.; Cui, X.; Wang, M.; Yao, X.; Xu, S. Anomalous Temperature-Dependent Exciton-Phonon Coupling in Cesium Lead Bromide Perovskite Nanosheets. *J. Phys. Chem. C* **2019**, *123*, 5128−5135.
(32) Bohn, B. J.; Tong, Y.; Gramlich, M.; Lai, M. L.; Döblinger, M.; Wang, K.; Hoye, R. L. Z.; Müller-Buschbaum, P.; Stranks, S. D.; Urban, A. S.; et al. Boosting Tunable Blue Luminescence of Halide Perovskite Nanoplatelets through Postsynthetic Surface Trap Repair. *Nano Lett.* **2018**, *18*, 5231−5238.
(33) Wei, K.; Chen, R.; Jiang, T.; Cheng, X.; Zheng, X.; Xu, Z. Temperature-Dependent Excitonic Photoluminescence Excited by Two-Photon Absorption in Perovskite $CsPbBr_3$ Quantum Dots. *Opt. Lett.* **2016**, *41*, 3821−3824.
(34) Lee, J.; Koteles, E. S.; Vassell, M. O. Luminescence Linewidths of Excitons in GaAs Quantum Wells below 150 K. *Phys. Rev. B: Condens. Matter Mater. Phys.* **1986**, *33*, 5512−5516.
(35) Gerlach, B.; Luczak, F. Ground-State energy of an Exciton-(LO) Phonon System in Two and Three Dimensions: General Outline and Three-Dimensional Case. *Phys. Rev. B: Condens. Matter Mater. Phys.* **1996**, *54*, 12841−12851.
(36) Wu, Y.; Li, J.; Ding, H.; Gao, Z.; Wu, Y.; Pan, N.; Wang, X. Negative Thermal Quenching of Photoluminescence in Annealed ZnO-Al_2O_3 Core-Shell Nanorods. *Phys. Chem. Chem. Phys.* **2015**, *17*, 5360−5365.
(37) Shibata, H. Negative Thermal Quenching Curves in Photoluminescence of Solids. *JPN. J. Appl. Phys.* **1998**, *37*, 550−553.
(38) Ossau, W. J.; Suris, R. *Optical Properties of 2D Systems with Interacting Electrons*; Springer: Berlin, 2003.
(39) Choi, J. H.; Cui, P.; Lan, H.; Zhang, Z. Linear Scaling of the Exciton Binding Energy versus the Band Gap of Two-Dimensional Materials. *Phys. Rev. Lett.* **2015**, *115*, 066403.

DOI: 10.1021/acs.jpcc.9b08606
J. Phys. Chem. C 2019, 123, 28893−28897